# PHILOSOPHICAL TRANSACTIONS A

royalsocietypublishing.org/journal/rsta

# Research



**Cite this article:** Wen B, Ding Z, Chini GP, Kerswell RR. 2022 Heat transport in Rayleigh—Bénard convection with linear marginality. *Phil. Trans. R. Soc. A* **380**: 20210039.

https://doi.org/10.1098/rsta.2021.0039

Received: 1 September 2021 Accepted: 6 December 2021

One contribution of 14 to a theme issue 'Mathematical problems in physical fluid dynamics (part 1)'.

#### **Subject Areas:**

applied mathematics, fluid mechanics

#### **Keywords:**

convection, instabilities, optimization

#### **Author for correspondence:**

Baole Wen

e-mail: baolew@umich.edu

# Heat transport in Rayleigh—Bénard convection with linear marginality

Baole Wen<sup>1</sup>, Zijing Ding<sup>2</sup>, Gregory P. Chini<sup>3,4</sup> and Rich R. Kerswell<sup>5</sup>

<sup>1</sup>Department of Mathematics, University of Michigan, Ann Arbor, MI 48109, USA

<sup>2</sup>School of Energy Science and Engineering, Harbin Institute of Technology, Harbin, Heilongjiang 150001, People's Republic of China <sup>3</sup>Integrated Applied Mathematics Program, and <sup>4</sup>Department of Mechanical Engineering, University of New Hampshire, Durham, NH 03824, USA

<sup>5</sup>Department of Applied Mathematics and Theoretical Physics, Centre for Mathematical Sciences, University of Cambridge, Cambridge CB3 OWA, UK

(D) BW, 0000-0003-2073-1508; GPC, 0000-0001-5539-3364; RRK, 0000-0001-5460-5337

Recent direct numerical simulations (DNS) and computations of exact steady solutions suggest that the heat transport in Rayleigh-Bénard convection (RBC) exhibits the classical 1/3 scaling as the Rayleigh number  $Ra \rightarrow \infty$  with Prandtl number unity, consistent with Malkus-Howard's marginally stable boundary layer theory. Here, we construct conditional upper and lower bounds for heat transport in twodimensional RBC subject to a physically motivated marginal linear-stability constraint. The upper estimate is derived using the Constantin-Doering-Hopf (CDH) variational framework for RBC with stress-free boundary conditions, while the lower estimate is developed for both stress-free and no-slip boundary conditions. The resulting optimization problems are solved numerically using a timestepping algorithm. Our results indicate that the upper heat-flux estimate follows the same 5/12 scaling as the rigorous CDH upper bound for the twodimensional stress-free case, indicating that the linear-stability constraint fails to modify boundary-layer thickness of the mean temperature profile. By contrast, the lower estimate successfully captures the 1/3 scaling for both

royalsocietypublishing.org/journal/rsta *Phil. Trans. R. Soc. A* **380**: 20210039

the stress-free and no-slip cases. These estimates are tested using marginally-stable equilibrium solutions obtained under the quasi-linear approximation, steady roll solutions and DNS data. This article is part of the theme issue 'Mathematical problems in physical fluid dynamics (part 1)'.

#### 1. Introduction

Understanding how a fluid convectively transfers heat between two isothermal horizontal parallel plates with the upper colder than the lower remains a canonical problem in fluid mechanics with hugely diverse applications in nature and industrial processes. The most fundamental issue is predicting the heat flux between the plates realized as a function of the controlling parameters of the problem: the Rayleigh Ra and Prandtl Pr numbers. The large Ralimit, where the flow is convectively turbulent, is particularly relevant and in the continuing absence of any full predictive theory the focus naturally has been on identifying a scaling law dependence of the Nusselt number, Nu—the ratio of the total heat flux to the conductive heat flux, with Ra. Generally, laboratory experiments and direct numerical simulations (DNS) of turbulent convection are consistent with  $Nu \sim Ra^{1/3}$  when the confining plates disallow any flow through them or the internal heating is limited within the boundary layers [1–5], although there are some competing claims of higher flux [6-8]: see [9-13] for recent commentaries. Theoretical estimates have varied from the so-called 'ultimate' regime  $Nu \sim Ra^{1/2}$  [14] (possibly with logarithmic corrections [15,16] and confirmed as a rigorous upper bound for the Boussinesq equations [17,18]) to the 'classical' scaling  $Nu \sim Ra^{1/3}$  predicted by other researchers (Priestley [19] argued that the heat flux should become independent of the layer separation if the temperature adjustment occurs entirely over the boundary layers; Howard [20] appealed to a marginally stable boundary layer idea; and Malkus [21] introduced a maximal heat transport hypothesis—see Spiegel [22] for a subsequent interpretation and statement of the specific prediction  $Nu \approx 0.07 Ra^{1/3}$  for the no-slip case). All exact steady Boussinesq solutions computed so far exhibit this classical scaling [10,23-27].

One way out of this uncertainty is to try to lower the scaling exponent in the upper bound on the heat flux to a value below that characterizing the 'ultimate' regime (i.e. 1/2). The way to do this seems clear: incorporate more dynamical constraints from the governing Boussinesq equations to restrict the set of fields over which the heat flux is maximized, but frustratingly no progress has been achieved so far [28–33] unless some key simplification is made. For example, it can be proved that  $Nu \le Ra^{5/12}$  in two-dimensional stress-free convection [34,35] and  $Nu \le Ra^{1/3}$  up to logarithms in the limit of infinite Pr [36,37]. For three-dimensional convection with no-slip plates at finite Pr, the best bound is still the nearly-two-decade-old 'ultimate' result  $Nu < 1 + 0.026Ra^{1/2}$  [38] (the corresponding result for stress-free plates being  $Nu < 1 + 0.055Ra^{1/2}$  [32]; see Goluskin & Doering [39] for a similar result for rough plates).

One distinct possibility is that the upper bound can *not* be lowered from the 'ultimate' regime scaling because there are perfectly good solutions (e.g. steady states) of the governing equations that achieve this heat flux scaling. These solutions are, however, never permanently realized as they are unstable so the observed heat flux is lower. In this case, no amount of extra constraints derived directly from the governing equations can lower the bound (Childress *et al.* [40] gives an example of this predicament in shear flow; see also Fantuzzi *et al.* [41] for a discussion). Indeed, a non-trivial lower bound on the heat flux cannot be derived precisely for this reason—the conductive state remains a solution as  $Ra \to \infty$ , so Nu = 1 is possible for all Ra in a perfect experiment (i.e. in the absence of noise). The concept of stability is clearly the missing ingredient, yet it is unclear how to rigorously formulate this notion as a constraint. We nevertheless pursue this idea here but lower our sights somewhat by considering only a physically plausible stability constraint that is not directly derivable from the equations. The

ensuing 'bound' is then admittedly conditional: it only holds for flow solutions obeying the stability constraint. Our purpose here, however, is to see if this hybrid approach of rigorous constraints married with some physical insight actually yields good estimates for the empirically observed heat flux. Moreover, this approach has additional utility: if the conditional bound is violated then the extra heuristic constraint is definitely not satisfied by the realized solution (see Kerswell [42] for a prior study in this spirit examining the relevant turbulent lengthscales active parallel to the plates in convection and Bouillaut *et al.* [43] which treats convection with internal heat sources and sinks in this themed issue).

We explore two stability constraints here using two-dimensional Rayleigh–Bénard convection as the testing ground. One is used to try to reduce the best existing upper bound [35] and the other to develop a conditional *lower* bound on the heat flux. These constraints are both marginal linear-stability constraints on the mean temperature profile (the mean flow is zero) but, crucially, are oppositely directed: one tests for the loss of stability (the upper bound) while the other for the lack of instability (the lower bound). Technically, the approach is to take the mean fields, ignore the fluctuation fields which sustain them (appealing to some smallness or rapid variation argument), and then examine whether small disturbances will grow or decay on these mean fields only (see equations (3.1)–(3.3)). This approach is widely used in the study of turbulent shear flows to try to rationalize the coherent structures that are observed (e.g. [44,45]). With no mean velocity field, here the constraint simply requires a linear stability calculation about the mean temperature field.

In the upper bound problem, the optimizing solution is clearly recognized to have overly thin boundary layers, which yield artificially elevated heat-flux bounds. These boundary layers are likely linearly stable yet should destabilize if allowed to thicken further through diffusion [20,46,47]. Hence, the logical stability constraint to apply here is one of loss of linear stability of the mean temperature profile: imposing this constraint while simultaneously maximizing the heat flux should realize the thinnest thermal layer which is marginally stable. From the perspective of the background method [18], the key point is that requiring the mean temperature profile to be marginally linearly stable restricts the degeneracy between the background and mean temperature profiles ( $\bar{\theta}$  below) and in so doing changes the objective functional to be minimized (see the end of §4 for a more detailed discussion). This calculation represents an attempt to formalize the argument of Howard [20] with the enticing possibility of achieving the 'classical' exponent of 1/3.

In the lower bound problem for the heat flux, as noted above, it is well known that the conductive state remains a valid solution to the governing equations yet, as Ra is increased, this conduction temperature profile becomes increasingly more linearly unstable and is certainly not realized in any physical experiment. Hence an obvious stability constraint on the mean temperature gradient for a lower bound is to require that it is not dynamically unstable, with marginal stability following if the constraint is active. This constraint on the mean temperature field is not to be confused with the linear stability of any convective solution (mean+fluctuation part) with respect to the full governing equations. Any such solution, stable or unstable, is considered for the lower heat-flux estimate provided the associated mean temperature profile is not linearly unstable.

The reminder of this paper is organized as follows. The equations governing Rayleigh–Bénard convection are stated in the next section. In §3, the marginal linear-stability constraint is introduced and formulated as a Rayleigh quotient. This constraint is then imposed on the mean temperature profile in §4 and §5 to construct, respectively, the upper and lower heat-flux estimates (i.e. the conditional bounds). The quasi-linear reduction for two-dimensional Rayleigh–Bénard convection is also introduced in §5 to verify the lower estimate. Solutions for the upper estimates, lower estimates and quasi-linear dynamical equilibria are computed numerically using simple time-stepping methods (see appendix A). Our results, including comparisons with the exact steady (roll) solutions and data from direct numerical simulations, are presented in §6, and our conclusions are given in §7.

royalsocietypublishing.org/journal/rsta Phil. Trans. R. Soc. A **380**: 20210039

#### 2. Problem formulation

We consider the dimensionless Boussinesq equations governing Rayleigh–Bénard convection in a two-dimensional fluid layer (in the x–z plane) that is heated from below and cooled from above:

$$\frac{1}{Pr}(\partial_t \mathbf{u} + \mathbf{u} \cdot \nabla \mathbf{u}) = -\nabla p + \nabla^2 \mathbf{u} + Ra\hat{\mathbf{z}}T,$$
(2.1)

$$\nabla \cdot \mathbf{u} = 0 \tag{2.2}$$

and

$$\partial_t T + \mathbf{u} \cdot \nabla T = \nabla^2 T,\tag{2.3}$$

where  $\mathbf{u} = u\hat{x} + w\hat{z}$  is the velocity field, p is the pressure and T is the temperature. In the dimensionless spatial domain  $(x,z) \in [0,\Gamma] \times [0,1]$ , all fields are taken to be  $\Gamma$ -periodic in x. At the lower and upper walls (i.e. z=0,1), the temperature is held fixed at 1 and 0, respectively, and the velocity field satisfies no-penetration and stress-free boundary conditions

$$T = 1 \& w = \partial_z u = 0$$
 at  $z = 0$ ;  $T = 0 \& w = \partial_z u = 0$  at  $z = 1$ , (2.4)

or no-slip boundary conditions

$$T = 1 \& w = u = 0$$
 at  $z = 0$ ;  $T = 0 \& w = u = 0$  at  $z = 1$ . (2.5)

Three control parameters govern the system: the domain aspect ratio  $\Gamma$ , the Prandtl number  $Pr = \nu/\kappa$ , the ratio of the kinematic viscosity  $\nu$  to the thermal diffusivity  $\kappa$  of the fluid, and the Rayleigh number  $Ra = \alpha g \Delta T h^3/(\nu \kappa)$ , the ratio of driving to damping forces, where  $\alpha$  is the thermal expansion coefficient, g is the gravitational acceleration,  $\Delta T$  is the dimensional temperature drop from the bottom boundary to the top one, and h is the layer thickness. The Nusselt number is defined as the ratio of the heat transport in the presence of convective motion to the conductive heat transport in the absence of fluid motion

$$Nu = 1 + \lim_{\widetilde{t} \to \infty} \frac{1}{\widetilde{t}} \int_{0}^{\widetilde{t}} \langle wT \rangle \, \mathrm{d}t, \tag{2.6}$$

where the angle brackets denote a spatial average, i.e. for some function *f* 

$$\langle f \rangle \equiv \frac{1}{\Gamma} \int_{0}^{1} \int_{0}^{\Gamma} f \, \mathrm{d}x \mathrm{d}z.$$
 (2.7)

The equations of motion imply the equivalent expression [48]

$$Nu = \lim_{\tilde{t} \to \infty} \frac{1}{\tilde{t}} \int_0^{\tilde{t}} ||\nabla T||^2 dt,$$
 (2.8)

where  $||f|| \equiv \langle |f|^2 \rangle^{1/2}$ .

The evolution equation for the (negative) scalar vorticity  $\Omega = \partial w/\partial x - \partial u/\partial z$  can be derived by taking the curl of equation (2.1)

$$\frac{1}{P_r}(\partial_t \Omega + \mathbf{u} \cdot \nabla \Omega) = \nabla^2 \Omega + Ra\partial_x T, \tag{2.9}$$

where  $\Omega|_{z=0,1} = 0$  for the case of stress-free boundary conditions.

# 3. Linear-marginality constraint

We begin by introducing the linear stability constraint and expressing the result as a Rayleigh quotient. The governing equations linearized about the general mean base state,  $T_B(z) \& \mathbf{U}_B(z) = \mathbf{0}$ 

royalsocietypublishing.org/journal/rsta Phil. Trans. R. Soc. A **380**: 2021003s

(so  $\Omega_B = 0$ ) are

$$\partial_t \theta = -w \partial_z T_B + \nabla^2 \theta, \tag{3.1}$$

$$\nabla \cdot \mathbf{u} = 0 \tag{3.2}$$

and

$$\frac{1}{Pr}\partial_t \Omega = \nabla^2 \Omega + Ra\partial_x \theta, \tag{3.3}$$

where  $\theta$ ,  $\mathbf{u}$  and  $\Omega$  are small-amplitude disturbances to the temperature, velocity and vorticity fields, respectively. We introduce a stream function  $\psi$  to describe the fluid motion so that  $(u, w) = (\partial_z \psi, -\partial_x \psi)$  and  $\nabla^2 \psi = -\Omega$ . Then, the linearized equations (3.1) and (3.3) can be expressed as

$$\partial_t \theta = \partial_x \psi \, \partial_z T_B + \nabla^2 \theta \tag{3.4}$$

and

$$\frac{1}{Pr}\partial_t(\nabla^2\psi) = -Ra\partial_x\theta + \nabla^4\psi,\tag{3.5}$$

where the above disturbance equations are solved subject to

$$\theta = 0 \& \psi = \partial_z^2 \psi = 0 \quad \text{at } z = 0 \text{ and } 1$$
 (3.6)

for stress-free boundaries and

$$\theta = 0 \& \psi = \partial_z \psi = 0 \text{ at } z = 0 \text{ and } 1,$$
 (3.7)

for no-slip boundaries.

Since the linearized system is autonomous in time, the time-dependence of the small perturbations can be taken to be proportional to  $e^{-\lambda_l t}$ . The resulting linear-stability eigenvalue problem is

$$-\nabla^2 \theta - \partial_z T_B \partial_x \psi = \lambda_I \theta \tag{3.8}$$

and

$$Ra\partial_x \theta - \nabla^4 \psi = \lambda_l \frac{1}{p_r} \nabla^2 \psi, \tag{3.9}$$

where the infinitesimal perturbation decays exponentially in time if the real part of  $\lambda_l$ ,  $\Re(\lambda_l)$ , is *positive*. In matrix form, equations (3.8)–(3.9) become

$$L\mathbf{v} = \lambda_l M \mathbf{v},\tag{3.10}$$

where

$$L = \begin{bmatrix} -\nabla^2 & -\partial_z T_B \partial_x \\ Ra \partial_x & -\nabla^4 \end{bmatrix}; \quad \mathbf{v} = \begin{bmatrix} \theta(x, z) \\ \psi(x, z) \end{bmatrix} \quad \text{and} \quad M = \begin{bmatrix} \mathbf{I} & 0 \\ 0 & \frac{1}{P_r} \nabla^2 \end{bmatrix}. \tag{3.11}$$

In this investigation, we construct upper and lower heat-flux estimates subject to a marginal linear-stability constraint on the ground state eigenvalue

$$\Re(\lambda_l^0) \ge 0. \tag{3.12}$$

Below we express the eigenvalue  $\lambda_l$  and its complex conjugate using Rayleigh quotients. Defining the inner product

$$(f,g) = \langle f^*g \rangle = \frac{1}{\Gamma} \int_0^1 \int_0^{\Gamma} f^*g \, dx dz,$$
 (3.13)

where f and g are vectors and the superscript '\*' denotes the complex conjugate, the adjoint of an operator F is obtained via

$$(F\mathbf{v}, \mathbf{v}^{\dagger}) = (\mathbf{v}, F^{\dagger}\mathbf{v}^{\dagger}), \tag{3.14}$$

where the superscript 't' denotes the adjoint. The adjoint operators of L and M, i.e.  $L^{\dagger}$  and  $M^{\dagger}$ , can be obtained using integration by parts, e.g.

$$(L\mathbf{v}, \mathbf{v}^{\dagger}) = \langle (-\nabla^{2}\theta^{*} - \partial_{z}T_{B}\partial_{x}\psi^{*})\theta^{\dagger} + (Ra\partial_{x}\theta^{*} - \nabla^{4}\psi^{*})\psi^{\dagger} \rangle$$
$$= \langle \theta^{*}(-\nabla^{2}\theta^{\dagger} - Ra\partial_{x}\psi^{\dagger}) + \psi^{*}(\partial_{z}T_{B}\partial_{x}\theta^{\dagger} - \nabla^{4}\psi^{\dagger}) \rangle.$$

royalsocietypublishing.org/journal/rsta Phil. Trans. R. Soc. A **380**: 20210039

Hence, the adjoint linear-stability eigenvalue problem is

$$L^{\dagger}\mathbf{v}^{\dagger} = \lambda_{I}^{\dagger}M^{\dagger}\mathbf{v}^{\dagger},\tag{3.15}$$

where

$$L^{\dagger} = \begin{bmatrix} -\nabla^2 & -Ra\partial_x \\ \partial_z T_B \partial_x & -\nabla^4 \end{bmatrix}; \quad \mathbf{v}^{\dagger} = \begin{bmatrix} \theta^{\dagger}(x, z) \\ \psi^{\dagger}(x, z) \end{bmatrix} \quad \text{and} \quad M^{\dagger} = \begin{bmatrix} \mathbf{I} & 0 \\ 0 & \frac{1}{Pr} \nabla^2 \end{bmatrix}. \tag{3.16}$$

Forming the appropriate Rayleigh quotients, we obtain

$$\lambda_{l} = \frac{(\mathbf{v}^{\dagger}, L\mathbf{v})}{(\mathbf{v}^{\dagger}, M\mathbf{v})}; \quad \lambda_{l}^{\dagger} = \frac{(\mathbf{v}, L^{\dagger}\mathbf{v}^{\dagger})}{(\mathbf{v}, M^{\dagger}\mathbf{v}^{\dagger})} = \frac{(L\mathbf{v}, \mathbf{v}^{\dagger})}{(M\mathbf{v}, \mathbf{v}^{\dagger})} = \lambda_{l}^{*}. \tag{3.17}$$

It has been proved by Spiegel [49] that  $\Im(\lambda_l) = 0$  when  $\Re(\lambda_l) \le 0$  for general  $T_B(z)$  for stress-free boundary conditions. As we focus on the marginal case in this study, below we assume that the ground state eigenvalue  $\lambda_l^0$  in equation (3.10) is real for all wavenumbers.<sup>1</sup> Then, the linear-marginality constraint (3.12) becomes

$$\lambda_l^0 \ge 0. \tag{3.18}$$

# 4. Upper heat-flux estimate based on linear marginality

In this section, we construct the upper heat-flux estimate subject to the marginal linear-stability constraint (3.18) within the Constantin–Doering–Hopf (CDH) variational framework. For brevity and simplicity, the implementation is performed only for the stress-free case.

We begin by decomposing the temperature field T(x, z, t) into a time-independent background profile  $\tau(z)$  plus an arbitrarily large perturbation  $\theta(x, z, t)$ 

$$T(x,z,t) = \tau(z) + \theta(x,z,t), \tag{4.1}$$

where  $\tau(0) = 1$ ,  $\tau(1) = 0$  and  $\theta(x, 0, t) = \theta(x, 1, t) = 0$ . Then, equation (2.3) becomes

$$\partial_t \theta + \mathbf{u} \cdot \nabla \theta = \nabla^2 \theta + \partial_z^2 \tau - w \partial_z \tau. \tag{4.2}$$

Following Whitehead & Doering [34,50], the equations of motion together with the background decomposition and the stress-free boundary conditions imply

$$\frac{1}{2}\frac{\mathrm{d}}{\mathrm{d}t}||\mathbf{u}||^2 = -Pr||\nabla \mathbf{u}||^2 + PrRa\langle w\theta \rangle,\tag{4.3}$$

$$||\nabla T||^2 = ||\nabla \theta||^2 + \int_0^1 [2\partial_z \tau \partial_z \overline{\theta} + (\partial_z \tau)^2] \, \mathrm{d}z,\tag{4.4}$$

$$\frac{1}{2}\frac{\mathrm{d}}{\mathrm{d}t}||\theta||^2 = -||\nabla\theta||^2 - \int_0^1 \partial_z \tau \,\partial_z \overline{\theta} \,\mathrm{d}z - \langle w\theta \,\partial_z \tau \rangle \tag{4.5}$$

and

$$\frac{1}{2}\frac{\mathrm{d}}{\mathrm{d}t}||\Omega||^2 = -Pr||\nabla\Omega||^2 + PrRa\langle\Omega\,\partial_x\theta\rangle,\tag{4.6}$$

where the overline denotes the horizontal average. As the infinite long-time averages of the left-hand sides of equations (4.3), (4.5) and (4.6) vanish, the Nusselt number Nu (2.8) can also be

 $<sup>^{1}</sup>$ This assumption is also verified using a standard optimization package for both no-slip and stress-free boundary conditions.

expressed as the following combination [34,51–53]:

$$Nu = \lim_{\tilde{t} \to \infty} \frac{1}{\tilde{t}} \int_{0}^{\tilde{t}} \left\{ \frac{b}{PrRa} (4.3) + (4.4) + c(4.5) + \frac{a}{PrRa^{3/2}} (4.6) \right\} dt$$

$$= \lim_{\tilde{t} \to \infty} \frac{1}{\tilde{t}} \int_{0}^{\tilde{t}} \left( nu - \frac{1}{1 - b} Q_{e} \right) dt, \tag{4.7}$$

where a, b and c are scalar 'balance' parameters for the enstrophy constraint and global energies, and

$$nu = \frac{1}{1 - b} \left[ \int_0^1 (\partial_z \tau)^2 dz - b + (c - 2) \int_0^1 \partial_z^2 \tau \overline{\theta} dz - (c - 1) \int_0^1 (\partial_z \overline{\theta})^2 dz \right]$$
(4.8)

and

$$Q_{e} = \left\langle (c-1)|\nabla \tilde{\theta}|^{2} + \frac{a}{Ra^{3/2}}|\nabla \Omega|^{2} + \frac{b}{Ra}\Omega^{2} + c\partial_{z}\tau w\tilde{\theta} - \frac{a}{Ra^{1/2}}\Omega \partial_{x}\tilde{\theta} \right\rangle, \tag{4.9}$$

where  $\tilde{\theta} = \theta - \overline{\theta}$  and  $\overline{\tilde{\theta}} = 0$ . If we can choose the background profile  $\tau(z)$  and coefficients a > 0, 0 < b < 1 and c > 1 so that  $Q_e \ge 0$  for all functions  $\tilde{\theta} = \tilde{\theta}(x,z)$ ,  $\Omega = \Omega(x,z)$  and w = w(x,z) satisfying periodic boundary conditions in x and homogeneous Dirichlet conditions in z and the local constraint  $\nabla^2 w = \partial_x \Omega$ , then nu is an upper bound on Nu. Minimizing nu subject to the energy spectral constraint  $Q_e \ge 0$  yields the optimal upper bound in the CDH framework. It should be noted that the positivity constraint for the quadratic form  $Q_e \ge 0$  is equivalent to the non-negativity of the ground state eigenvalue  $\lambda_e^0$  of the self-adjoint problem [35]

$$-2\nabla^2 \tilde{\theta} + \frac{c}{c-1} w \partial_z \tau + \frac{a}{Ra^{1/2}(c-1)} \partial_x \Omega = \lambda_e \tilde{\theta}, \tag{4.10}$$

$$-\frac{2a}{Ra^{3/2}}\nabla^2\Omega + \frac{2b}{Ra}\Omega - \frac{a}{Ra^{1/2}}\partial_x\tilde{\theta} + \partial_x\gamma = \lambda_e\Omega$$
 (4.11)

$$\nabla^2 \gamma + c\tilde{\theta} \partial_z \tau = 0 \tag{4.12}$$

and

$$\nabla^2 w - \partial_x \Omega = 0, (4.13)$$

where the Lagrange-multiplier field  $\gamma(x, z)$  enforcing the local constraint (4.13) satisfies periodic boundary conditions in x and homogeneous Dirichlet conditions in z.

Below we impose the marginal linear-stability constraint (3.18) on the mean temperature profile  $\overline{T} = \tau + \overline{\theta}$  within the CDH framework. The Lagrange functional corresponding to this optimization problem can be expressed as

$$\mathcal{L} = nu - \left\langle (c - 1)|\nabla \tilde{\theta}|^2 + \frac{a}{Ra^{3/2}}|\nabla \Omega|^2 + \frac{b}{Ra}\Omega^2 + c\partial_z \tau w \tilde{\theta} - \frac{a}{Ra^{1/2}}\Omega \partial_x \tilde{\theta} \right\rangle - \left\langle \gamma(\nabla^2 w - \partial_x \Omega) \right\rangle - d\lambda_l^0, \tag{4.14}$$

where the (positive) term 1/(1-b) from equation (4.7) is omitted for simplification without affecting the optimal upper bound as we pursue the marginality of  $\mathcal{Q}_e$ , d is a scalar Lagrange multiplier related to the linear-stability constraint and  $\lambda_l^0$  is assumed to be real as discussed in §3. The variables  $\tau$ ,  $\overline{\theta}$ , a, b and c are determined by minimizing nu, subject to the energy spectral constraint  $\mathcal{Q}_e \geq 0$  (i.e.  $\lambda_e^0 \geq 0$ ) and the linear-stability constraint  $\lambda_l^0 \geq 0$ . From §3,

$$d\lambda_{l}^{0} = d\frac{\langle \mathbf{v}^{\dagger *} L \mathbf{v} \rangle}{\langle \mathbf{v}^{\dagger *} M \mathbf{v} \rangle} = d\frac{\langle \theta_{l}^{\dagger *} [-\nabla^{2} \theta_{l} - \partial_{z} (\tau + \overline{\theta}) \partial_{x} \psi_{l}] + \psi_{l}^{\dagger *} (Ra \partial_{x} \theta_{l} - \nabla^{4} \psi_{l}) \rangle}{\langle \theta_{l}^{\dagger *} \theta_{l} + \psi_{l}^{\dagger *} \frac{1}{P_{r}} \nabla^{2} \psi_{l} \rangle},$$

$$= Ra^{-1} \langle \theta_{l}^{\dagger *} [-\nabla^{2} \theta_{l} - \partial_{z} (\tau + \overline{\theta}) \partial_{x} \psi_{l}] + \psi_{l}^{\dagger *} (Ra \partial_{x} \theta_{l} - \nabla^{4} \psi_{l}) \rangle, \tag{4.15}$$

oyalsocietypublishing.org/journal/rsta Phil. Trans. R. Soc. A **380**: 2021003

where the eigenfunctions  $\theta_l$  and  $\psi_l$  and their adjoints for the linear-stability eigenvalue problem are normalized so that  $\langle \theta_l^{\dagger *}\theta_l + \psi_l^{\dagger *}(1/Pr)\nabla^2\psi_l \rangle = dRa$ . Then, equation (4.14) can be written as

$$\mathcal{L} = nu - \left\langle (c-1)|\nabla \tilde{\theta}|^2 + \frac{a}{Ra^{3/2}}|\nabla \Omega|^2 + \frac{b}{Ra}\Omega^2 + c\partial_z \tau w \tilde{\theta} - \frac{a}{Ra^{1/2}}\Omega \partial_x \tilde{\theta} \right\rangle - \left\langle \gamma(\nabla^2 w - \partial_x \Omega) \right\rangle - Ra^{-1} \langle \theta_l^{\dagger *} [-\nabla^2 \theta_l - \partial_z (\tau + \overline{\theta}) \partial_x \psi_l] + \psi_l^{\dagger *} (Ra\partial_x \theta_l - \nabla^4 \psi_l) \rangle.$$
(4.16)

The first variations (Frechet derivatives) of this functional with respect to  $\tau$ ,  $\bar{\theta}$ ,  $\tilde{\theta}$ ,  $\Omega$ , w,  $\gamma$ , a, b, c,  $\theta_l^{\dagger *}$ ,  $\psi_l^{\dagger *}$ ,  $\theta_l$  and  $\psi_l$  (i.e.  $\delta \mathcal{L}/\delta \tau = 0$ ,  $\delta \mathcal{L}/\delta \tilde{\theta} = 0$ , etc.) yield the Euler–Lagrange equations

$$-\partial_z^2 \tau + \frac{2(c-1)(1-b)}{c} \partial_z (\overline{w\tilde{\theta}}) + \frac{1-b}{cRa} \partial_z (\overline{\theta_l^{\dagger *}} \partial_x \psi_l) = 0, \tag{4.17}$$

$$-\partial_z^2 \overline{\theta} - \frac{(c-2)(1-b)}{c} \partial_z (\overline{w} \widetilde{\theta}) - \frac{1-b}{cRa} \partial_z (\overline{\theta_l^{\dagger *}} \partial_x \psi_l) = 0, \tag{4.18}$$

$$-2\nabla^2 \tilde{\theta} + \frac{c}{c-1} w \partial_z \tau + \frac{a}{Ra^{1/2}(c-1)} \partial_x \Omega = 0, \tag{4.19}$$

$$-\frac{2a}{Ra^{3/2}}\nabla^2\Omega + \frac{2b}{Ra}\Omega - \frac{a}{Ra^{1/2}}\partial_x\tilde{\theta} + \partial_x\gamma = 0,$$
(4.20)

$$\nabla^2 \gamma + c\tilde{\theta} \, \partial_z \tau = 0, \tag{4.21}$$

$$\nabla^2 w - \partial_x \Omega = 0, \tag{4.22}$$

$$-\left\langle \frac{1}{Ra^{3/2}} |\nabla \Omega|^2 - \frac{1}{Ra^{1/2}} \Omega \partial_x \tilde{\theta} \right\rangle = 0, \tag{4.23}$$

$$b - 1 + \left\{ \frac{Ra\left(\int_0^1 (\partial_z \tau)^2 dz - 1 + (c - 2)\int_0^1 \partial_z^2 \tau \overline{\theta} dz - (c - 1)\int_0^1 (\partial_z \overline{\theta})^2 dz\right)}{\langle \Omega^2 \rangle} \right\}^{1/2} = 0, \quad (4.24)$$

$$\left\langle \frac{1}{1-b} \left[ \partial_z^2 \tau \overline{\theta} - (\partial_z \overline{\theta})^2 \right] - (|\nabla \widetilde{\theta}|^2 + \widetilde{\theta} w \partial_z \tau) \right\rangle = 0, \tag{4.25}$$

$$-\nabla^2 \theta_l - \partial_z (\tau + \overline{\theta}) \partial_x \psi_l = 0, \tag{4.26}$$

$$Ra\partial_x \theta_l - \nabla^4 \psi_l = 0, \tag{4.27}$$

$$-\nabla^2 \theta_l^{\dagger} - Ra \partial_x \psi_l^{\dagger} = 0 \tag{4.28}$$

and

$$\partial_z(\tau + \overline{\theta})\partial_x\theta_l^{\dagger} - \nabla^4\psi_l^{\dagger} = 0. \tag{4.29}$$

The relationship between the linear-stability eigenfunctions and their adjoints for marginal modes will be discussed in the next section. After taking an x-derivative and rescaling, we can rewrite equation (4.20) as

$$-2\nabla^{2}(\partial_{x}\Omega) + \frac{2b}{a}Ra^{1/2}\partial_{x}\Omega - Ra\partial_{x}^{2}\tilde{\theta} + \frac{Ra^{3/2}}{a}\partial_{x}^{2}\gamma = 0.$$
 (4.30)

Since  $\langle \Omega \cdot \delta \mathcal{L} / \delta \Omega \rangle = 0$ , namely

$$\left\langle -\frac{2a}{Ra^{3/2}}|\nabla\Omega|^2 - \frac{2b}{Ra}\Omega^2 + \frac{a}{Ra^{1/2}}\Omega\partial_x\tilde{\theta} - \Omega\partial_x\gamma \right\rangle = 0, \tag{4.31}$$

hence from equation (4.23), equation (4.31) becomes

$$a = \frac{Ra^{3/2} \langle \gamma \, \partial_x \Omega \rangle - 2bRa^{1/2} \langle \Omega^2 \rangle}{\langle |\nabla \Omega|^2 \rangle}.$$
 (4.32)

Solving the Euler-Lagrange equations (4.17)-(4.19), (4.30), (4.21), (4.22), (4.32) and (4.24)-(4.27) subject to the energy spectral constraint  $\lambda_e^0 \ge 0$  and the linear-stability constraint  $\lambda_I^0 \ge 0$  yields the

optimal mean temperature  $\overline{T} = \tau + \overline{\theta}$  and the upper estimate  $Nu_{cdhl} = nu$ . At this point, it is worth clarifying the effect of the linear stability constraint. Setting c = 2

for illustrative purposes, the objective functional to be maximized over  $\overline{\theta}$  (to construct an upper

bound) and minimized over  $\tau$  subject to the energy spectral constraint (4.9) (to obtain the lowest upper bound) is then simply

$$nu = \frac{1}{1-b} \left[ \int_0^1 (\partial_z \tau)^2 - (\partial_z \overline{\theta})^2 dz - b \right]. \tag{4.33}$$

In the absence of the linear stability constraint, the Euler–Lagrange equation (4.18) forces  $\overline{\theta}=0$ . With the linear stability constraint,  $\overline{\theta}$  can no longer vanish and the objective functional is necessarily reduced. A reasonable estimate of the size of this reduction can be made by assuming a piecewise-linear profile for  $\overline{T}$  with boundary layers of thickness  $O(Ra^{-1/3})$  (and zero interior gradient following Howard [20]) and the background profile with the usual boundary layers of thickness  $O(Ra^{-1/2})$  to be marginally energy stable. Then

$$\int_{0}^{1} (\partial_{z}\tau)^{2} - (\partial_{z}\overline{\theta})^{2} dz = \int_{0}^{1} \partial_{z}\overline{T}(2\partial_{z}\tau - \partial_{z}\overline{T}) dz = O(Ra^{1/3}).$$
(4.34)

implying  $nu \sim Ra^{1/3}$  rather than the usual  $Ra^{1/2}$ . This simple estimate motivated the numerical treatment of the full variational problem.

#### 5. Lower heat-flux estimate based on linear marginality

Next, we construct the lower heat-flux estimate subject to the marginal linear-stability constraint (3.18) for both the stress-free and no-slip scenarios. Given the time- and horizontally averaged temperature profile

$$\overline{\overline{T}}(z) = \lim_{\tilde{t} \to \infty} \frac{1}{\tilde{t}} \int_{0}^{\tilde{t}} \frac{1}{\Gamma} \int_{0}^{\Gamma} T(x, z, t) \, \mathrm{d}x \, \mathrm{d}t, \tag{5.1}$$

the perturbation temperature is defined so that  $\theta(x,z,t) = T(x,z,t) - \overline{\overline{T}}(z)$  and  $\overline{\overline{\theta}} = 0$ . Then, equation (2.8) gives

$$Nu = \lim_{\tilde{t} \to \infty} \frac{1}{\tilde{t}} \int_{0}^{\tilde{t}} ||\nabla \theta||^{2} dt + \int_{0}^{1} (\partial_{z} \overline{T})^{2} dz \ge \int_{0}^{1} (\partial_{z} \overline{T})^{2} dz.$$
 (5.2)

A rigorous albeit trivial lower bound of  $Nu \ge 1$  for Rayleigh–Bénard convection is achieved by the conduction solution  $\overline{\overline{T}} = 1 - z$ . In this section, however, we seek a better lower estimate by using the marginal linear-stability constraint (3.18) on  $\overline{\overline{T}}$  to exclude the conduction solution, i.e. by minimizing  $\int_0^1 (\partial_z \overline{\overline{T}})^2 \, \mathrm{d}z$  subject to  $\lambda_I^0 \ge 0$ . To compute the optimal  $\overline{\overline{T}}$  efficiently, we work directly with the corresponding Euler–Lagrange equations derived by identifying a Lagrange functional for this optimization problem

$$\mathcal{L} = \int_{0}^{1} (\partial_{z} \overline{\overline{T}})^{2} dz - d\lambda_{l}^{0}$$

$$= \int_{0}^{1} (\partial_{z} \overline{\overline{T}})^{2} dz - d\frac{\langle \mathbf{v}^{\dagger *} L \mathbf{v} \rangle}{\langle \mathbf{v}^{\dagger *} M \mathbf{v} \rangle}$$

$$= \int_{0}^{1} (\partial_{z} \overline{\overline{T}})^{2} dz - d\frac{\langle \mathbf{v}^{\dagger *} L \mathbf{v} \rangle}{\langle \mathbf{v}^{\dagger *} M \mathbf{v} \rangle}$$

$$= \int_{0}^{1} (\partial_{z} \overline{\overline{T}})^{2} dz - d\frac{\langle \mathbf{v}^{\dagger *} (-\nabla^{2} \theta - \partial_{z} \overline{\overline{T}} \partial_{x} \psi) + \psi^{\dagger *} (Ra \partial_{x} \theta - \nabla^{4} \psi) \rangle}{\langle \theta^{\dagger *} \theta + \psi^{\dagger *} \frac{1}{P_{r}} \nabla^{2} \psi \rangle}, \tag{5.3}$$

where the first term in  $\mathcal{L}$  is the objective functional to be minimized, d is a scalar Lagrange multiplier related to the linear-stability constraint and  $\lambda_l^0$  is assumed to be real (see §3). We then

royalsocietypublishing.org/journal/rsta Phil. Trans. R. Soc. A **380**: 2021003:

normalize the eigenfunctions by setting  $\langle \theta^{\dagger *} \theta + \psi^{\dagger *} \frac{1}{p_r} \nabla^2 \psi \rangle = d$ , so equation (5.3) becomes

$$\mathcal{L} = \int_0^1 (\partial_z \overline{\overline{T}})^2 dz - \langle \theta^{\dagger *} (-\nabla^2 \theta - \partial_z \overline{\overline{T}} \partial_x \psi) + \psi^{\dagger *} (Ra \partial_x \theta - \nabla^4 \psi) \rangle. \tag{5.4}$$

The first variations of this functional with respect to  $\overline{\overline{T}}$ ,  $\theta^{+*}$ ,  $\psi^{+*}$ ,  $\theta$  and  $\psi$  (i.e.  $\delta \mathcal{L}/\delta \overline{\overline{T}} = 0$ ,  $\delta \mathcal{L}/\delta \theta^{+*} = 0$ , etc.), respectively, yield the Euler–Lagrange equations

$$-2\partial_z^2 \overline{\overline{T}} - \partial_z (\overline{\theta^{\dagger *}} \partial_x \psi) = 0, \tag{5.5}$$

$$-\nabla^2 \theta - \partial_z \overline{\overline{T}} \partial_x \psi = 0, \tag{5.6}$$

$$Ra\partial_x \theta - \nabla^4 \psi = 0, \tag{5.7}$$

$$-\nabla^2 \theta^{\dagger} - Ra \partial_x \psi^{\dagger} = 0 \tag{5.8}$$

and

$$\partial_z \overline{\overline{T}} \partial_x \theta^{\dagger} - \nabla^4 \psi^{\dagger} = 0, \tag{5.9}$$

where equations (5.6) and (5.7) correspond to the marginally stable version of the direct eigenvalue problem (3.8) and (3.9), and correspondingly for equations (5.8) and (5.9) for the adjoint problem.

The solution to equations (5.5)–(5.9) can be obtained by expressing

$$\theta = \sum_{n=1}^{N} \hat{\theta}_n(z) \sin(nkx), \quad \psi = \sum_{n=1}^{N} \hat{\psi}_n(z) \cos(nkx)$$
 (5.10)

and

$$\theta^{\dagger} = \sum_{n=1}^{N} \hat{\theta}_{n}^{\dagger}(z) \sin(nkx), \quad \psi^{\dagger} = \sum_{n=1}^{N} \hat{\psi}_{n}^{\dagger}(z) \cos(nkx), \tag{5.11}$$

where n is the horizontal mode number, N is a suitably large truncation index and  $k = 2\pi/\Gamma$  is the fundamental wavenumber. Equations (5.6)–(5.9) indicate that

$$\hat{\theta}_n = [D^2 - (nk)^2]\hat{\psi}_n^{\dagger} \text{ and } \hat{\psi}_n = \hat{\theta}_n^{\dagger},$$
 (5.12)

where  $D \equiv d/dz$ . Then substituting equations (5.10)–(5.12) into equations (5.5)–(5.7) gives

$$-2D^{2}\overline{T} + \frac{1}{2}D\sum_{n=1}^{N}(nk\hat{\psi}_{n}^{2}) = 0,$$
(5.13)

$$-[D^{2} - (nk)^{2}]\hat{\theta}_{n} + D\overline{\overline{T}}(nk)\hat{\psi}_{n} = 0$$
(5.14)

and

$$-[D^2 - (nk)^2]^2 \hat{\psi}_n + Ra(nk)\hat{\theta}_n = 0.$$
 (5.15)

Solving the Euler–Lagrange equations (5.13)–(5.15) subject to the marginal linear-stability constraint  $\lambda_l^0 \ge 0$  yields the optimal mean temperature profile  $\overline{\overline{T}}$  and the lower estimate  $Nu_l = \int_0^1 (\partial_z \overline{\overline{T}})^2 dz$ .

In the next section, we provide a partial validation of our lower heat-flux estimate using marginally stable thermal equilibria (MSTE) computed under a quasi-linear (QL) reduction of the two-dimensional Boussinesq equations for Rayleigh–Bénard convection between no-slip boundaries [54]. Below we show that the steady-state QL approximation has a mathematical form similar to the Euler–Lagrange equations (5.5)–(5.7) for the lower heat-flux estimate.

The QL reduction begins with a decomposition of the temperature field into the horizontal-mean profile  $\overline{T}$  plus a perturbation  $\theta$ ,

$$T(x,z,t) = \overline{T}(z,t) + \theta(x,z,t), \tag{5.16}$$

with  $\bar{\theta} = 0$ . The horizontal mean of the velocity (or the stream function) vanishes due to incompressibility and symmetry. The horizontal mean of equation (2.3) then can be written as

$$\partial_t \overline{T} - \partial_z^2 \overline{T} - \partial_z (\overline{\theta} \partial_x \psi) = 0. \tag{5.17}$$

Under the QL approximation, the nonlinear terms  $\mathbf{u} \cdot \nabla \theta$  and  $\mathbf{u} \cdot \nabla \mathbf{u}$  are omitted from the perturbation equations, yielding

$$\partial_t \theta = \partial_x \psi \, \partial_z \overline{T} + \nabla^2 \theta \tag{5.18}$$

and

$$\frac{1}{Pr}\partial_t(\nabla^2\psi) = -Ra\partial_x\theta + \nabla^4\psi,\tag{5.19}$$

which corresponds to the eigenvalue problem (3.8)–(3.9) upon setting  $T_B=\overline{T}$ . It is evident that equations (5.5)–(5.7) for the lower heat-flux estimate and the *steady* QL approximation (equations (5.17)–(5.19) with time-derivatives suppressed) share the same perturbation equations and similar mean equations for  $\overline{T}$  and  $\overline{T}$ . Crucially,  $Nu_l=\int_0^1 (\partial_z \overline{T})^2 \, \mathrm{d}z$  is a rigorous lower bound for  $Nu_{ql}=-\partial_z \overline{T}|_{z=0}$  for MSTE under the QL approximation as the latter automatically satisfies the marginal linear-stability constraint.

#### 6. Results

Downloaded from https://royalsocietypublishing.org/ on 25 April 2022

Following previous investigations [35,53,55,56], we solve the Euler–Lagrange equations derived in the preceding sections numerically using a simple time-stepping algorithm. The upper heatflux estimate proposed in §4 is computed for the stress-free case, while the lower estimate proposed in §5 is computed for both the stress-free and no-slip cases. To validate the lower estimate, we also compute marginally stable thermal equilibria under the QL approximation using a modified time-stepping method for both stress-free and no-slip scenarios. Details of the numerical methods and data are reported in appendix A. Since these solutions are time-independent,  $\overline{T}$  will be used below to denote the time- and horizontally-averaged temperature profile. The subscripts 'cdh', 'cdhl', 'ql' and 'l' hereafter refer to, respectively, the standard (rigorous) CDH framework, the CDH framework under the marginal linear-stability constraint (the upper estimate), the quasi-linear approximation, and the formalism for the lower heat-flux estimate, which only enforces linear marginality. Note that the results from all these schemes are Pr-independent.

Figure 1 shows the mean temperature profile  $\overline{T}(z)$ , the background profile  $\tau(z)$ , and the corresponding lowest branch of eigenvalues for  $Ra = 10^7$  and  $\Gamma = 2\sqrt{2}$  with stress-free boundary conditions. The profiles and eigenvalues are computed using the various schemes delineated above. For piecewise-linear  $\overline{T}$  with homogenized interior  $(\overline{T} \sim 1/2)$  [34], the energy spectral constraint  $\lambda_{\ell} \ge 0$  is stronger than the linear-stability constraint  $\lambda_{l} \ge 0$  and thereby generates a thinner boundary layer<sup>2</sup>: accordingly, any temperature profile satisfying the energy spectral constraint also satisfies the linear-stability constraint. In the CDH scheme, the energy spectral constraint is imposed on the background profile  $\tau(z)$ , which controls the boundary-layer thickness of  $\overline{T} = \tau + \overline{\theta}$  (figure 1*a*-*c*); however,  $\overline{T}$  develops a slightly unstable gradient in the interior offsetting the 'linear stability' of the boundary layer (figure 1a,d). In the CDHL scheme, the linearstability constraint produces an indistinguishable change to the background profile  $\tau$  (figure 1b) so that the boundary layer in  $\overline{T}$  and the energy spectra are negligibly affected (figure 1a,c); nevertheless, the interior gradient of  $\overline{T}$  is modified to ensure the linear marginality of the entire z-dependent profile (figure 1a,d). In both the CDH and CDHL schemes,  $\overline{\theta}$  in equation (4.8) adjusts to maximize nu to form an upper bound on Nu. Hence, even upon enforcing the linear-stability constraint, the CDHL scheme still 'pursues' the maximum possible transport by preserving the boundary-layer structure of  $\tau$  in  $\overline{T}$ . By contrast, the QL reduction and lower-estimate scheme

<sup>&</sup>lt;sup>2</sup>At large Ra, the boundary-layer thickness  $\delta$  under the energy spectral constraint scales as  $Ra^{-5/12}$  [34], while  $\delta$  under the linear-stability constraint scales as  $Ra^{-1/3}$  [20].

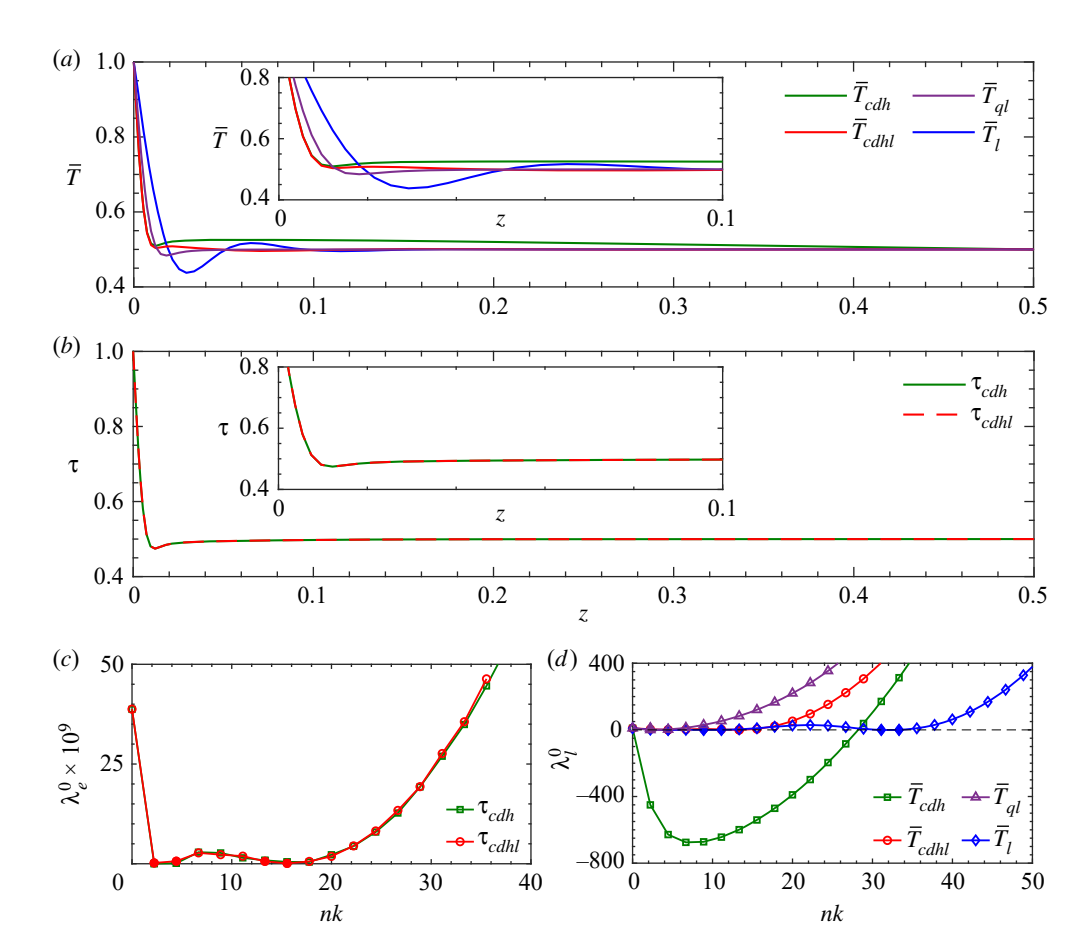


**Figure 1.** (a) Mean temperature profile  $\overline{I}$ , (b) background profile  $\tau$  and (c,d) ground state eigenvalue  $\lambda^0$  for  $Ra=10^7$  and  $\Gamma=2\sqrt{2}$  with stress-free boundary conditions. In (a,b), only half of the profile is plotted due to the antisymmetry about the mid-plane, and the insets show details of the profiles near the lower wall; in (c,d),  $\lambda_e^0$  and  $\lambda_f^0$  are computed via solving the eigenvalue problems (4.10)–(4.13) and (3.8)–(3.9) using  $\tau$  and  $\overline{I}$ , respectively.  $\tau$  and  $\overline{I}$  are marginally stable at certain critical wavenumbers  $n_c k$  with filled symbols. (Online version in colour.)

only impose linear marginality on  $\overline{T}$ , yielding a profile with a homogenized interior and thicker boundary layers (figure 1a,d).

Figure 2 shows the bifurcation of the critical wavenumbers  $n_c k$  as a function of Ra extracted from the computation of the lower heat-flux estimate. Interestingly, at large Ra the largest two critical wavenumbers scale as  $Ra^{1/3}$  for both the stress-free and no-slip cases, consistent with the scaling of the largest critical wavenumber arising under the steady QL approximation with no-slip boundary conditions as computed by O'Connor *et al.* [54]. We note that for steady roll solutions of the full Boussinesq equations, the rising/falling plumes adjacent to the edges of the convection cell are of thickness  $O(Ra^{-1/3})$  [23,26]. Under the QL approximation with stress-free boundary conditions, however, our computations indicate that at  $\Gamma = 2\sqrt{2}$  there exists only one critical mode at  $n_c = 1$  up to  $Ra = 10^9$ , i.e. only the single critical wavenumber  $n_c k = k = \pi/\sqrt{2}$ .

Figure 3 shows the collapse of the temperature profiles near the lower wall (z=0) at large Ra. For all schemes, the temperature is strongly homogenized in the interior with  $\overline{T} \sim 1/2$ . For the upper (CDHL) estimate with stress-free boundary conditions, the boundary layer is dominated by the energy spectral constraint so the thickness scales as  $Ra^{-5/12}$  (figure 3a), consistent with the CDH result [35,53]. For the steady QL solution and lower heat-flux estimate, however, the computations shown in figure 3b-d and those by O'Connor et al. [54] indicate the thickness of

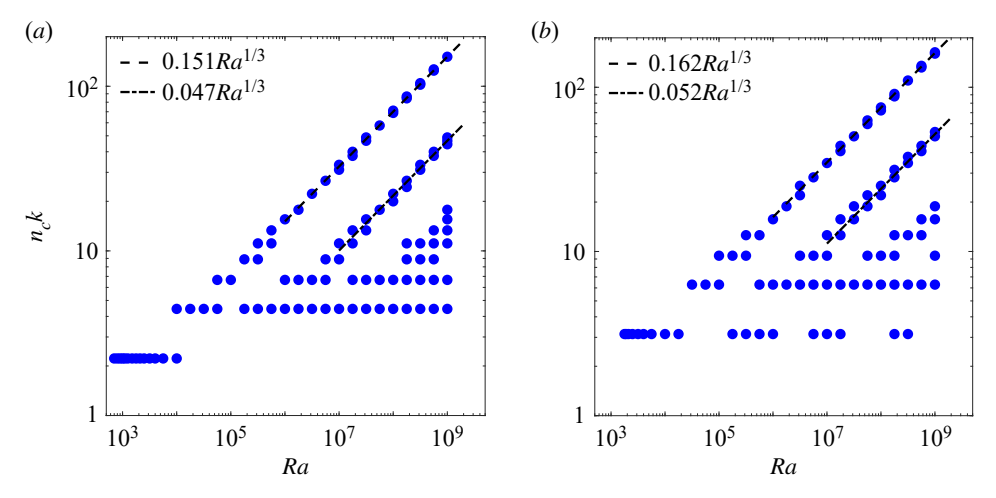


**Figure 2.** Bifurcation diagram showing the critical wavenumbers  $n_c k$  of marginal modes from the computation of the lower heat-flux estimate as a function of Ra. (a)  $\Gamma = 2\sqrt{2}$  with stress-free boundary conditions; (b)  $\Gamma = 2$  with no-slip boundary conditions. The critical wavenumbers of the highest two branches scale as  $Ra^{1/3}$  at large Ra. (Online version in colour.)

the temperature profile scales as  $Ra^{-1/3}$  for both stress-free and no-slip boundary conditions, consistent with the exact steady roll solutions of the full Boussinesq equations [26,27].

Figure 4 shows the dependence of the compensated Nusselt number on Ra for the various schemes with stress-free boundary conditions. For stress-free Rayleigh–Bénard convection, the conduction state becomes linearly unstable as Ra exceeds the critical value  $Ra_c = 8\pi^4 \approx 779$  with the corresponding critical wavelength  $\Gamma_c = 2\sqrt{2}$ . As discussed above, in the CDHL scheme the marginal linear-stability constraint drives an unstable mean temperature gradient in the interior, instead of thickening the boundary layer. Consequently, the upper estimate  $Nu_{cdhl}$  follows the 5/12 scaling, i.e.  $Nu_{cdhl} \sim 0.106Ra^{5/12}$ , and the reduction in the upper bound is minimal. On the contrary, simply enforcing the linear-stability constraint on  $\overline{T}$  under the lower-estimate scheme yields the 1/3 scaling at large Ra, i.e.  $Nu_l \sim 0.137Ra^{1/3}$ . This lower estimate also holds for the MSTE solutions under the QL approximation, i.e.  $Nu_l \leq Nu_{ql}$ , as the latter, by construction, satisfies the marginal linear-stability constraint; specifically,  $Nu_{ql} \sim 0.295Ra^{1/3}$  lies slightly more than a factor of 2 above the lower estimate. Note that although  $Nu_{ql}$  lies strictly below  $Nu_{cdh}$  in figure 4, it is an open question whether the latter is a rigorous upper bound for the heat flux achieved by steady solutions to the QL system.

To further test the upper and lower heat-flux estimates, we compare these estimates with the DNS data for 'non-shearing' convection with Pr=1 and  $\Gamma=2$  from Goluskin et~al. [57], and with the steady roll solutions for Pr=1 and  $\Gamma=2\sqrt{2}$  computed using a spectral solver developed by Wen et~al. [26] and predicted using matched asymptotic analysis of the fully nonlinear Boussinesq equations in the limit  $Ra\to\infty$  by Chini & Cox [23]. At small Ra, the upper bound  $Nu_{cdh}$  is saturated by steady rolls; at large Ra, heat transport from both DNS and steady roll solutions increases towards the 1/3 scaling, within a factor of 2 of the lower estimate. We have confirmed that  $\overline{T}$  from the steady roll solutions satisfies the linear-stability constraint  $\lambda_l^0 \ge 0$ , so the Nu achieved by these solutions must lie between the lower and upper estimates. It should be noted, however, that in the stress-free case there also exist shearing modes of convection in which the sheared mean flow breaks the linear-stability constraint: Nu is greatly reduced and violates the lower estimate [57].

Figure 5 shows the dependence of the compensated Nu on Ra for the various schemes with noslip boundary conditions. For no-slip Rayleigh–Bénard convection, the conduction state becomes linearly unstable as Ra exceeds the critical value  $Ra_c \approx 1708$  with the corresponding critical wavelength  $\Gamma_c \approx 2.016$ . The best-known upper bound for finite Pr,  $Nu \sim 0.026Ra^{1/2}$  [38], is much higher than the Nu data reported in figure 5 at large Ra and therefore is not included in the

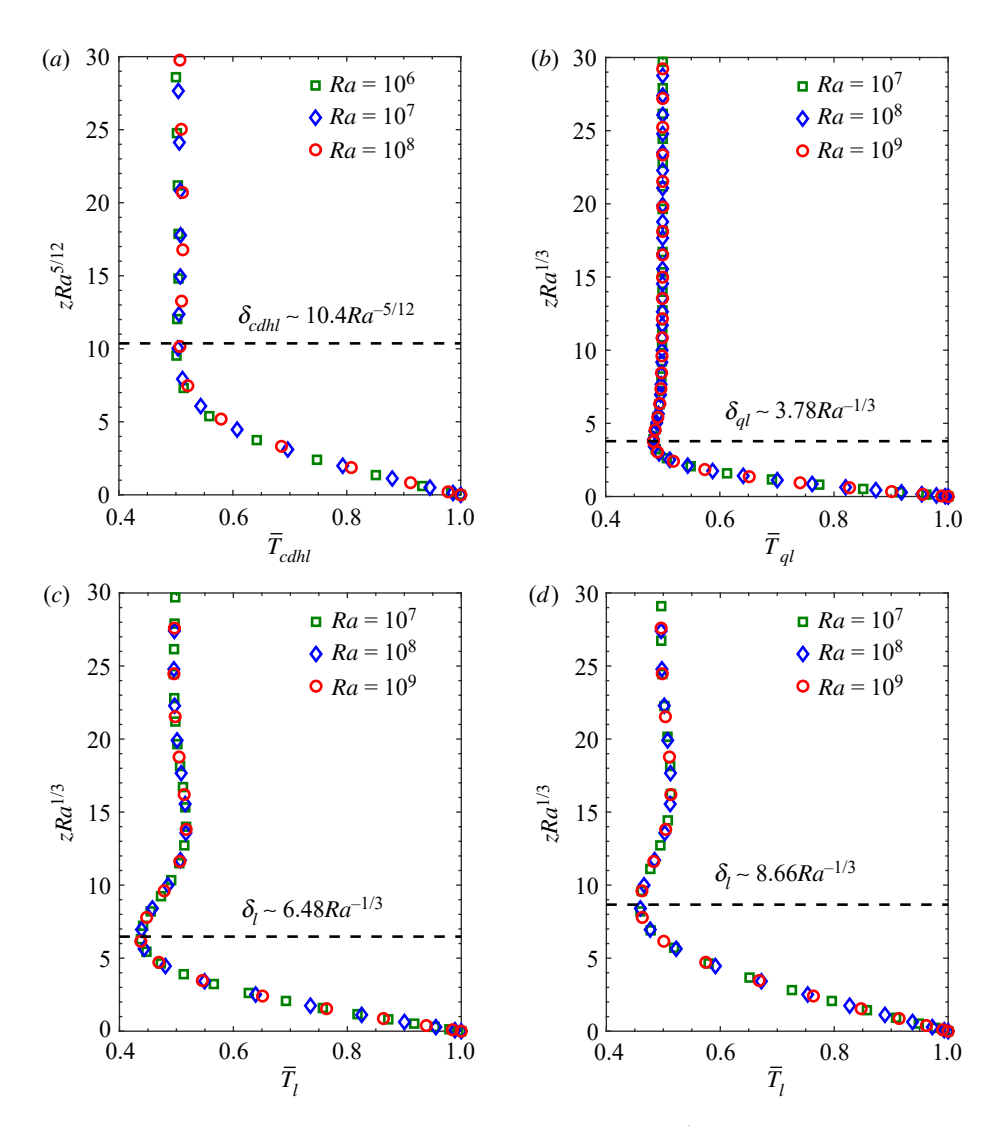


**Figure 3.** Scaled mean temperature profile  $\overline{I}$  near the lower wall. (a-c)  $\Gamma=2\sqrt{2}$  with stress-free boundary conditions; (d)  $\Gamma=2$  with no-slip boundary conditions. The dashed lines are used to denote the edges of the boundary layers—i.e. the first local extrema with  $\partial_z \overline{I}=0$  away from the boundary—for (a) the upper estimate (CDHL), (b) the QL approximation and (c,d) the lower estimate. (Online version in colour.)

plot. As shown in the figure, the steady QL solutions computed here agree precisely with the computations by O'Connor *et al.* [54] for  $Ra \in [10^5, 2 \times 10^6]$ . As in the stress-free case, at small Ra the Nu data from the QL solutions, DNS, and steady rolls collapse; at large Ra, Nu from all four schemes reported in figure 5 scales as  $Ra^{1/3}$ , although the convergence for the Nu-maximizing steady rolls and turbulent convection from DNS occurs at even larger Ra (around  $Ra = 10^{13}$ ). Specifically, as  $Ra \to \infty$ , Nu from the MSTE under the QL approximation, the lower estimate and Nu-maximizing steady rolls lies, respectively, within factors of 3.4, 2.6 and 2.2 of the DNS data. Obviously, the lower estimate holds for the steady QL solutions, but is violated by the Nu-maximizing steady rolls and turbulent convection at large Ra, indicating that the mean temperature profile is not linearly stable for those flows.

The no-slip lower estimate for the heat flux is  $Nu_l = 0.089Ra^{1/3}$ . This scaling and prefactor are fully consistent with the work of Currie [46] and Kerr [59] who both studied the linear stability of boundary-confined temperature profiles with no-slip conditions (these represent trial fields for

Phil. Trans. R. Soc. A 380: 20210039

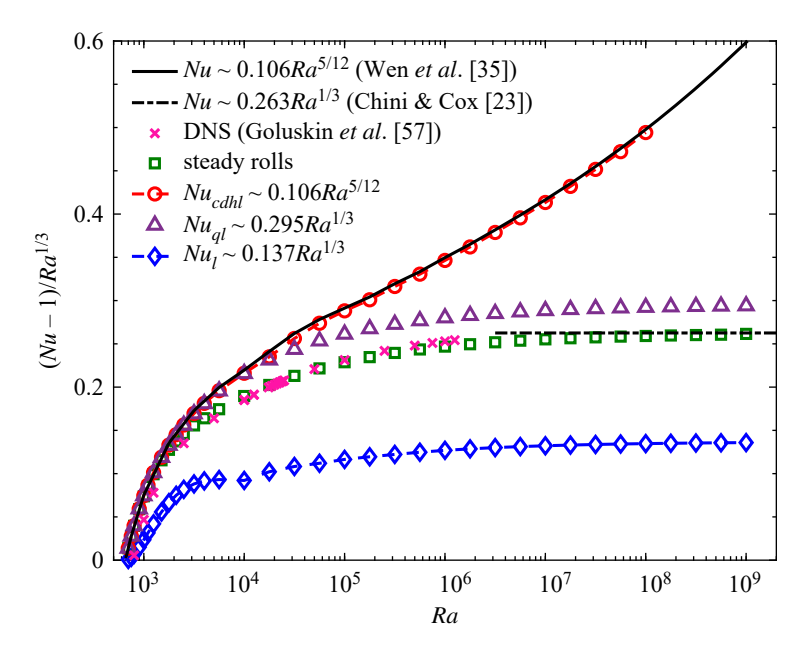


**Figure 4.** Dependence of compensated *Nu* on *Ra* under stress-free boundary conditions for: the upper (circles) and lower (diamonds) heat-flux estimates, steady QL solutions (triangles), numerical steady-roll solutions (squares) and the corresponding asymptotic prediction (dashed line) from Chini & Cox [23], DNS results (crosses) from Goluskin *et al.* [57] and rigorous upper bounds applying to all flows (solid line) from Wen *et al.* [35].  $\Gamma = 2$  and Pr = 1 for DNS data and  $\Gamma = 2\sqrt{2}$  for other data. The steady roll solutions are computed at Pr = 1 using the spectral solver developed by Wen *et al.* [26]. (Online version in colour.)

the minimization problem). Currie's temperature gradient is completely confined to a boundary layer and gives the better (lower) estimate from above of the minimum: in the limit of vanishing boundary layer thickness, he found numerically a critical boundary-layer Rayleigh number of 32 which corresponds to  $Nu = (Ra/32)^{1/3} \approx 0.315Ra^{1/3} > Nu_l$ . Kerr [59] treats the diffusive error function profile using a complementary matched asymptotic expansion approach and his results correspond to  $Nu = (Ra/\pi^2)^{1/3} / \sqrt{2} \approx 0.330Ra^{1/3} > Nu_l$ . Both estimates corroborate the classical scaling behaviour of our lower estimate.

#### 7. Conclusion

The best rigorous upper bounds on the heat transport in Rayleigh-Bénard convection remain stubbornly well above data obtained from DNS and laboratory experiments. The notion of dynamical stability seems to be a critical element missing from existing methods for obtaining rigorous bounds. Accordingly, in this study, we have introduced a novel hybrid approach in which a physically plausible—although not rigorously derivable—marginal linear-stability constraint is incorporated into variational formalisms for estimating the heat transport in two-dimensional Rayleigh-Bénard convection. Our (conditional) upper heat-flux estimate is constructed within the CDH variational framework for the stress-free case. A lower estimate also is obtained for both stress-free and no-slip scenarios. To obtain these conditional bounds, we first demonstrate how linear marginality can be imposed on the mean temperature profile through a Rayleigh quotient formulation, and then solve the resulting Euler-Lagrange equations numerically using efficient time-stepping algorithms. The computational results reveal that the improvement (i.e. the reduction in the bound) provided by the upper estimate is negligible, i.e.  $Nu_{cdhl} \lesssim Nu_{cdh} \sim 0.106 Ra^{5/12}$ . This reflects the fact that the linear-stability constraint is almost entirely accommodated by an adjustment of the interior gradient of  $\overline{T}_{cdh}$ , rendering it slightly unstable, rather than via the anticipated thickening of the thermal boundary layer. The lower estimate, however, does successfully capture the classical 1/3 scaling for both stress-free ( $Nu_l \sim$ 

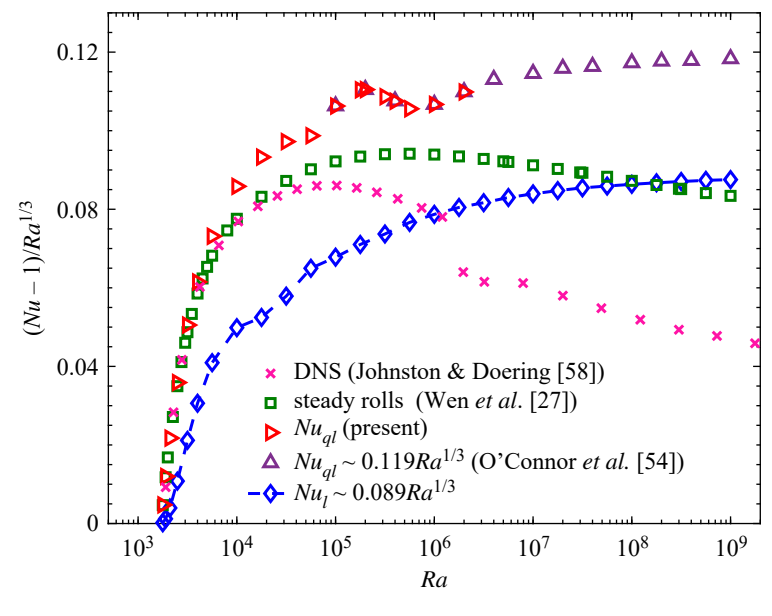


**Figure 5.** Dependence of compensated Nu on Ra under no-slip boundary conditions for: the lower heat-flux estimate (diamonds), steady QL solutions (triangles) and numerical steady-roll solutions with Nu-maximizing aspect ratios (squares) from Wen  $et\ al.$  [27], and DNS results (crosses) from Johnston & Doering [58].  $\Gamma=2$  for the lower heat-flux estimate and DNS and  $\Gamma=4$  for the QL solutions. Pr=1 for DNS and steady rolls. The QL solutions (right-pointing triangles) are computed using the time-stepping methods developed in this work. Here, the computations are performed up to  $Ra=2\times10^6$  to fill the gap between the convective onset and the O'Connor  $et\ al.$  data, which start at  $Ra=10^5$  [54], and also to verify our numerical algorithm at  $10^5 \le Ra \le 2\times10^6$ , while the high-Ra data can be obtained from O'Connor  $et\ al.$  [54]. For Nu-maximizing steady rolls,  $Nu\sim0.077Ra^{1/3}$  at  $Ra\gtrsim10^{13}$  [27]; for 2D turbulent convection from DNS,  $Nu\sim0.035Ra^{1/3}$  at  $Ra\gtrsim10^{13}$  [8,11]. (Online version in colour.)

Downloaded from https://royalsocietypublishing.org/ on 25 April 2022

 $0.137Ra^{1/3}$ ) and no-slip ( $Nu_l \sim 0.089Ra^{1/3}$ ) cases consistent with the marginally stable thermal equilibria (MSTE) computed under the quasi-linear approximation, the steady roll solutions and DNS data. These upper and lower estimates naturally hold for the MSTE, which must satisfy the linear-stability constraint, providing a partial validation of our formalism. For the stress-free case, the steady roll solutions also satisfy the linear-stability constraint, so the lower estimate underestimates their heat flux. By contrast, for the no-slip case, the linear-stability constraint is violated by Nu-maximizing steady rolls and by the turbulent convection. While the lower estimate actually overestimates the heat flux in these cases, it nevertheless exhibits the correct scaling with Ra, unlike available rigorous bounds.

The success of the lower estimate computed here at least in capturing the exponent if not the numerical prefactor for realized heat flux is encouraging and begs the question whether something similar would work in other problems (e.g. shear flow). The challenge is always to exclude the basic response of the flow which becomes dynamically unstable as the system forcing is increased. Incorporating a stability criterion in a lower estimate makes sense but, as formulated here, is somewhat arbitrary. The choice to consider the linear stability of the mean state is a plausible starting point but really needs to be extended to include more information about the optimal state. The optimal state is, of course, only an approximation to a steady solution of the governing equations but the hope is that adding a realistic stability constraint brings it closer to a *realized* solution.

Ultimately, the fundamental issue is that current upper bounding techniques discard the time derivatives in the governing equations by long-time-averaging and hence key information about dynamic stability is lost. A first stab at re-incorporating that has been made here. Disappointingly, this has not reflected Howard's idea of a marginally stable thermal boundary layer to give an

upper bound with classical scaling although, as some compensation, this scaling has emerged in our lower estimate. A more targeted stability criterion may well do better. There is no doubt that a more systematic approach clearly would be highly desirable and that much remains to be done if bounds are to be brought closer to observations.

Data accessibility. This article has no additional data.

Authors' contributions. R.R.K. initiated the research program and with B.W. and G.P.C. conceived of and designed the study. B.W. carried out the computations and data analysis. All authors drafted, read and approved the manuscript. B.W.: conceptualization, data curation, formal analysis, investigation, methodology, project administration, software, validation, visualization, writing—original draft, writing—review and editing; Z.D.: investigation, writing—review and editing; G.P.C.: conceptualization, formal analysis, investigation, methodology, project administration, supervision, writing—review and editing; R.R.K.: conceptualization, formal analysis, investigation, methodology, project administration, supervision, writing—original draft, writing—review and editing. All authors gave final approval for publication and agreed to be held accountable for the work performed therein.

Competing interests. The authors declare that they have no competing interests.

Funding. B.W. was supported by US National Science Foundation under grant no. DMS-1813003. Z.D. acknowledges the support of National Natural Science Foundation of China under grant no. 52176065.

Acknowledgements. We thank David Goluskin for helpful discussions and Charlie Doering for his 'unbounded' enthusiasm for all 'bounding' work. Charlie was a joyful teacher, enthusiastic supervisor and fantastic

collaborator, always encouraging us all to work harder to 'lower those bounds and make contact with the

data'. We dedicate this paper to his memory.

# Appendix A. Numerical methods and data

The schemes of upper estimate, quasi-linear approximation and lower estimate proposed in §4 and §5 yield the (Euler–Lagrange) equations with similar structures. These equations admit 'true' and 'spurious' solutions which are non-trivial at particular horizontal wavenumbers. The desired true solution satisfies the energy spectral constraint  $\lambda_e^0 \ge 0$  and/or the linear-stability constraint  $\lambda_l^0 \ge 0$  for all horizontal wavenumbers and seems to be unique. The existence of the spurious solutions is because the perturbation terms become trivial/inactive on some critical mode(s) (note that zero perturbations always satisfy the equations) so that the ground state eigenvalue  $\lambda^0$  becomes negative there (see detailed discussions in Wen *et al.* [35,55]). Some investigations use numerical continuation [32,38] or a semidefinite programming [60–65] to compute the optimal background profile by imposing the spectral constraint for all wavenumbers. In this work, we employ *simple* and *efficient* time-stepping methods to seek the true solution for various schemes discussed in §4 and §5. This numerical method was developed in Wen *et al.* [35,55] and successfully applied to porous media convection [55,56], Rayleigh–Bénard convection between stress-free boundaries [35,53], Taylor–Couette flow [66], and plane Couette flow with injection and suction [67].

For the upper-estimate scheme, we add pseudo-time derivatives  $\partial_T \tau$ ,  $\partial_T \overline{\theta}$ ,  $\partial_T \widetilde{\theta}$ ,  $\partial_T (\partial_x \Omega)$ ,  $\partial_T c$  and  $\partial_T \theta_l$  into equations (4.17)–(4.19), (4.30), (4.25) and (4.26), respectively,

$$\partial_{\mathcal{T}}\tau + \frac{\delta\mathcal{L}}{\delta\tau} = 0 \Rightarrow \partial_{\mathcal{T}}\tau - \partial_{z}^{2}\tau + \frac{2(c-1)(1-b)}{c}\partial_{z}(\overline{w\tilde{\theta}}) + \frac{1-b}{cRa}\partial_{z}(\overline{\theta_{l}^{\dagger*}}\partial_{x}\psi_{l}) = 0, \quad (A1)$$

$$\partial_{\mathcal{T}}\overline{\theta} - \frac{\delta\mathcal{L}}{\delta\overline{\theta}} = 0 \Rightarrow \partial_{\mathcal{T}}\overline{\theta} - \partial_{z}^{2}\overline{\theta} - \frac{(c-2)(1-b)}{c}\partial_{z}(\overline{w}\widetilde{\theta}) - \frac{1-b}{cRa}\partial_{z}(\overline{\theta_{l}^{\dagger*}}\partial_{x}\psi_{l}) = 0, \tag{A2}$$

$$\partial_{T}\tilde{\theta} - \frac{\delta \mathcal{L}}{\delta \tilde{\theta}} = 0 \Rightarrow \partial_{T}\tilde{\theta} - 2\nabla^{2}\tilde{\theta} + \frac{c}{c-1}w\partial_{z}\tau + \frac{a}{Ra^{1/2}(c-1)}\partial_{x}\Omega = 0, \tag{A3}$$

$$\partial_{\mathcal{T}}(\partial_{x}\Omega) - \frac{Ra^{3/2}}{a}\partial_{x}\frac{\delta\mathcal{L}}{\delta\Omega} = 0 \Rightarrow \partial_{\mathcal{T}}(\partial_{x}\Omega) - 2\nabla^{2}(\partial_{x}\Omega) + \frac{2b}{a}Ra^{1/2}\partial_{x}\Omega - Ra\partial_{x}^{2}\tilde{\theta}$$

$$+\frac{Ra^{3/2}}{a}\partial_x^2\gamma = 0, (A4)$$

royalsocietypublishing.org/journal/rsta Phil. Trans. R. Soc. A **380**: 20210039

$$\partial_{\mathcal{T}} c + \frac{\delta \mathcal{L}}{\delta c} = 0 \Rightarrow \partial_{\mathcal{T}} c + \left\langle \frac{1}{1 - b} [\partial_z^2 \tau \overline{\theta} - (\partial_z \overline{\theta})^2] - (|\nabla \tilde{\theta}|^2 + \tilde{\theta} w \partial_z \tau) \right\rangle = 0 \tag{A5}$$

and

$$\partial_{\mathcal{T}}\theta_{l} - Ra \frac{\delta \mathcal{L}}{\delta \theta_{l}^{+*}} = 0 \Rightarrow \partial_{\mathcal{T}}\theta_{l} - \nabla^{2}\theta_{l} - \partial_{z}(\tau + \overline{\theta})\partial_{x}\psi_{l} = 0. \tag{A 6}$$

For the quasi-linear approximation scheme, directly time-stepping the system yields unsteady computational results at large Ra. To prompt the time stepping to converge to a stationary solution, we drop the time-derivative terms and then add the pseudo-time derivative  $\partial_T \theta$  into the steady version of equation (5.18),

$$\partial_{\mathcal{T}}\theta - \nabla^2\theta - \partial_x\psi\,\partial_z\overline{T} = 0. \tag{A7}$$

For the lower-estimate scheme, we add pseudo-time derivatives  $\partial_T \overline{T}$  and  $\partial_T \theta$  into equations (5.5) and (5.6), respectively,

$$\partial_{\mathcal{T}} \overline{T} + \frac{\delta \mathcal{L}}{\delta \overline{T}} = 0 \Rightarrow \partial_{\mathcal{T}} \overline{T} - 2 \partial_{z}^{2} \overline{T} - \partial_{z} (\overline{\theta^{+*}} \partial_{x} \psi) = 0$$
 (A8)

and

$$\partial_{\mathcal{T}}\theta - \frac{\delta \mathcal{L}}{\delta \theta^{+*}} = 0 \Rightarrow \partial_{\mathcal{T}}\theta - \nabla^{2}\theta - \partial_{z}\overline{T}\partial_{x}\psi = 0. \tag{A 9}$$

Next, we advance the above 'time-dependent' equations until converging to a stationary solution, i.e. the solution of the original time-independent equations. In computations, a Fourier series in x and a Chebyshev collocation method in z are used for spatial discretization, while temporal discretization is achieved using the Crank–Nicolson method for the linear terms and a two-step Adams-Bashforth method for the nonlinear terms. It has been proved by Wen et al. [35] that in the CDH schemes with fixed balance parameters, the spurious solutions are linearly unstable in the time-dependent Euler-Lagrange systems for porous media convection, Rayleigh-Bénard convection between stress-free boundaries and plane Couette flow, while the true solution is linearly stable and therefore the global attractor. In our computations, to avoid converging to the spurious solutions, non-zero initial data are given for all potential critical modes (simply we use  $\overline{T}$  and perturbation terms from the first critical mode at a computed Ra as the initial condition); and as time evolves, the perturbations at non-critical modes decay to zero and the time-dependent systems converge to the true solution. To reduce the computations and speed up the convergence, during the time stepping, we check the spectral constraints and exclude the non-critical modes at which the perturbations are close to zero or  $\lambda^0 \gtrsim O(1)$ . In computations of upper heat-flux estimate, at moderate and large Ra we fix the balance parameters a, b and c for the first thousands of time steps to obtain a good initial guess of the solution, and then advance all the variables until reaching the convergence.

At large Ra, the convergence of the time-stepping method may be slow due to the small step size to maintain the numerical stability. The results from the time-stepping method provide a good initial guess for Newton's method with quadratic convergence rate, which is the second stage of the two-step algorithm proposed by Wen et al. [35,55]. In this study, as the computations are focused on  $Ra \le 10^8$  or  $Ra \le 10^9$  for various schemes, only the time-stepping method (the first stage) is used.

Table 1 gives numerical values of the Nusselt number Nu plotted in figures 4 and 5.

**Table 1.** Values of Nu plotted in figures 4 and 5 from the upper-estimate scheme (cdhl), the quasi-linear approximation scheme (ql), the lower-estimate scheme (l), and the steady roll solutions (s). The high-Ra  $Nu_{ql}$  data for the no-slip case can be found in O'Connor et al. [54].

|                    | stress free        |                  |                 |        | no slip          |                 |
|--------------------|--------------------|------------------|-----------------|--------|------------------|-----------------|
| Ra                 | Nu <sub>cdhl</sub> | Nu <sub>ql</sub> | Nu <sub>l</sub> | Nus    | Nu <sub>ql</sub> | Nu <sub>l</sub> |
| 700                | 1.1227             | 1.1227           | 1.0074          | 1.1227 | 1                | 1               |
| 750                | 1.2525             | 1.2524           | 1.0304          | 1.2522 | 1                | 1               |
| 800                | 1.3692             | 1.3691           | 1.0636          | 1.3684 | 1                | 1               |
| 900                | 1.5722             | 1.5720           | 1.1456          | 1.5695 | 1                | 1               |
| 10 <sup>3</sup>    | 1.7455             | 1.7443           | 1.2356          | 1.7386 | 1                | 1               |
| 1100               | 1.8953             | 1.8944           | 1.3254          | 1.8842 | 1                | 1               |
| 1250               | 2.0906             | 2.0893           | 1.4526          | 2.0702 | 1                | 1               |
| 1500               | 2.3616             | 2.3594           | 1.6374          | 2.3213 | 1                | 1               |
| 10 <sup>13/4</sup> | 2.6115             | 2.6086           | 1.8053          | 2.5453 | 1.0575           | 1.0023          |
| 2100               | 2.8574             | 2.8537           | 1.9602          | 2.7588 | 1.2784           | 1.0507          |
| 2500               | 3.1205             | 3.1161           | 2.1108          | 2.9813 | 1.4871           | 1.1466          |
| 10 <sup>14/4</sup> | 3.4887             | 3.4836           | 2.2934          | 3.2858 | 1.7416           | 1.3107          |
| 4000               | 3.8770             | 3.8715           | 2.4543          | 3.6035 | 1.9762           | 1.4860          |
| 10 <sup>15/4</sup> | 4.4836             | 4.4779           | 2.6567          | 4.1025 | 2.3003           | 1.7280          |
| 10 <sup>4</sup>    | 5.6544             | 5.6468           | 2.9848          | 5.0870 | 2.8493           | 2.0740          |
| 10 <sup>17/4</sup> | 7.1340             | 7.0379           | 3.6667          | 6.2851 | 3.4346           | 2.3692          |
| 10 <sup>18/4</sup> | 9.1021             | 8.7043           | 4.4236          | 7.7352 | 4.0745           | 2.8304          |
| 10 <sup>19/4</sup> | 11.491             | 10.709           | 5.2909          | 9.4913 | 4.7821           | 3.4894          |
| 10 <sup>5</sup>    | 14.374             | 13.125           | 6.4050          | 11.619 | 5.9328           | 4.1471          |
| 10 <sup>21/4</sup> | 17.923             | 16.044           | 7.7186          | 14.196 | 7.2086           | 4.9943          |
| 10 <sup>22/4</sup> | 22.549             | 19.573           | 9.3254          | 17.318 | 8.4025           | 6.0213          |
| 10 <sup>23/4</sup> | 28.284             | 23.842           | 11.295          | 21.101 | 9.7138           | 7.3271          |
| 10 <sup>6</sup>    | 35.641             | 29.010           | 13.693          | 25.684 | 11.668           | 8.8704          |
| 10 <sup>25/4</sup> | 44.857             | 35.267           | 16.583          | 31.236 |                  | 10.749          |
| 10 <sup>26/4</sup> | 56.592             | 42.845           | 20.095          | 37.963 |                  | 12.987          |
| 10 <sup>27/4</sup> | 71.350             | 52.024           | 24.341          | 46.113 |                  | 15.757          |
| 10 <sup>7</sup>    | 90.059             | 63.142           | 29.484          | 55.985 |                  | 19.080          |
| 10 <sup>29/4</sup> | 113.76             | 76.610           | 35.724          | 67.946 |                  | 23.121          |
| 10 <sup>30/4</sup> | 143.82             | 92.926           | 43.278          | 82.437 |                  | 28.020          |
| 10 <sup>31/4</sup> | 181.88             | 112.69           | 52.437          | 99.993 |                  | 33.913          |
| 10 <sup>8</sup>    | 230.39             | 136.64           | 63.526          | 121.26 |                  | 41.080          |
| 10 <sup>33/4</sup> |                    | 165.65           | 76.965          | 147.03 |                  | 49.776          |
| 10 <sup>34/4</sup> |                    | 200.80           | 93.245          | 178.25 |                  | 60.316          |
| 10 <sup>35/4</sup> |                    | 243.38           | 112.97          | 216.09 |                  | 73.106          |
| 10 <sup>9</sup>    |                    | 294.97           | 136.87          | 262.51 |                  | 88.544          |

royalsocietypublishing.org/journal/rsta

Phil. Trans. R. Soc. A 380: 20210039

#### References

- 1. Niemela JJ, Skrbek L, Swanson C, Hall S, Sreenivasan KR, Donnelly RJ. 2000 New results in cryogenic helium flows at ultra-high Reynolds and Rayleigh numbers. *J. Low Temp. Phys.* **121**, 417–422. (doi:10.1023/A:1017505931073)
- Urban P, Musilová V, Skrbek L. 2011 Efficiency of heat transfer in turbulent Rayleigh-Bénard convection. *Phys. Rev. Lett.* 107, 014302. (doi:10.1103/PhysRevLett.107.014302)
- 3. Bouillaut V, Lepot S, Aumaître S, Gallet B. 2019 Transition to the ultimate regime in a radiatively driven convection experiment. *J. Fluid Mech.* **861**, R5. (doi:10.1017/jfm.2018.972)
- 4. Iyer KP, Scheel JD, Schumacher J, Sreenivasan KR. 2020 Classical 1/3 scaling of convection holds up to  $Ra = 10^{15}$ . *Proc. Natl Acad. Sci. USA* **117**, 7594–7598. (doi:10.1073/pnas.1922794117)
- Kawano K, Motoki S, Shimizu M, Kawahara G. 2021 Ultimate heat transfer in 'wall-bounded' convective turbulence. J. Fluid Mech. 914, A13. (doi:10.1017/jfm.2020.867)
- 6. Chavanne X, Chilla F, Chabaud B, Castaing B, Hebral B. 2001 Turbulent Rayleigh–Bénard convection in gaseous and liquid He. *Phys. Fluids* **13**, 1300–1320. (doi:10.1063/1.1355683)
- 7. He X, Funfschilling D, Nobach H, Bodenschatz E, Ahlers G. 2012 Transition to the ultimate state of turbulent Rayleigh–Bénard convection. *Phys. Rev. Lett.* **108**, 024502. (doi:10.1103/PhysRevLett.108.024502)
- 8. Zhu X, Mathai V, M. Stevens RJA, Verzicco R, Lohse D. 2018 Transition to the ultimate regime in two-dimensional Rayleigh–Bénard convection. *Phys. Rev. Lett.* **120**, 144502. (doi:10.1103/PhysRevLett.120.144502)
- 9. Chillà F, Schumacher J. 2012 New perspectives in turbulent Rayleigh–Bénard convection. *Eur. Phys. J. E* **35**, 58. (doi:10.1140/epje/i2012-12058-1)
- Waleffe F, Boonkasame A, Smith LM. 2015 Heat transport by coherent Rayleigh–Bénard convection. *Phys. Fluids* 27, 051702. (doi:10.1063/1.4919930)
- 11. Doering CR, Toppaladoddi S, Wettlaufer JS. 2019 Absence of evidence for the ultimate regime in two-dimensional Rayleigh–Bénard convection. *Phys. Rev. Lett.* **123**, 259401. (doi:10.1103/PhysRevLett.123.259401)
- 12. Doering CR. 2020 Absence of evidence for the ultimate state of turbulent Rayleigh–Bénard convection. *Phys. Rev. Lett.* **124**, 229401. (doi:10.1103/PhysRevLett.124.229401)
- 13. Doering CR. 2020 Turning up the heat in turbulent thermal convection. *Proc. Natl Acad. Sci. USA* **117**, 9671–9673. (doi:10.1073/pnas.2004239117)
- 14. Spiegel EA. 1963 A generalization of mixing-length theory of turbulent convection. *Ap. J.* **138**, 216–225. (doi:10.1086/147628)
- 15. Kraichnan RH. 1962 Turbulent thermal convection at arbitrary Prandtl number. *Phys. Fluids* 5, 1374–1389. (doi:10.1063/1.1706533)
- 16. Chavanne X, Chilla F, Castaing B, Hebral B, Chabaud B, Chaussy J. 1997 Observation of the ultimate regime in Rayleigh–Bénard convection. *Phys. Rev. Lett.* **79**, 3648–3651. (doi:10.1103/PhysRevLett.79.3648)
- 17. Howard LN. 1963 Heat transport by turbulent convection. *J. Fluid Mech.* 17, 405–432. (doi:10.1017/S0022112063001427)
- 18. Doering CR, Constantin P. 1996 Variational bounds on energy dissipation in incompressible flows. III. Convection. *Phys. Rev. E* **53**, 5957–5981. (doi:10.1103/PhysRevE.53.5957)
- 19. Priestley CHB. 1954 Convection from a large horizontal surface. Aus. J. Phys. 7, 176–201. (doi:10.1071/PH540176)
- 20. Howard LN. 1964 Convection at high Rayleigh number. *Applied Mechanics, Proc. of the Eleventh Int. Congress of Applied Mechanics, Munich*, pp. 1109–1115.
- 21. Malkus WVR. 1954 The heat transport and spectrum of thermal turbulence. *Proc. R. Soc.* **A225**, 196–212.
- 22. Spiegel EA. 1962 On the Malkus theory of turbulence. *Mecanique de la turbulence, Centre National de la Recherche Scientifique, Paris*, pp. 181–201.
- Chini GP, Cox SM. 2009 Large Rayleigh number thermal convection: Heat flux predictions and strongly nonlinear solutions. *Phys. Fluids* 21, 083603. (doi:10.1063/1.3210777)
- 24. Sondak D, Smith LM, Waleffe F. 2015 Optimal heat transport solutions for Rayleigh–Bénard convection. *J. Fluid Mech.* **784**, 565–595. (doi:10.1017/jfm.2015.615)
- 25. Motoki S, Kawahara G, Shimizu M. 2021 Multi-scale steady solution for Rayleigh–Bénard convection. *J. Fluid Mech.* **914**, A14. (doi:10.1017/jfm.2020.978)
- 26. Wen B, Goluskin D, LeDuc M, Chini GP, Doering CR. 2020 Steady Rayleigh–Bénard convection between stress-free boundaries. *J. Fluid Mech.* **905**, R4. (doi:10.1017/jfm.2020.812)

royalsocietypublishing.org/journal/rsta *Phil. Trans. R. Soc. A* **380**: 20210039

- 27. Wen B, Goluskin D, Doering CR. 2022 Steady Rayleigh–Bénard convection between no-slip boundaries. *J. Fluid Mech.* **933**, R4. (doi:10.1017/jfm.2021.1042)
- 28. Ierley GR, Worthing RA. 2001 Bound to improve: a variational approach to convective heat transport. *J. Fluid Mech.* 441, 223–253. (doi:10.1017/S0022112001004839)
- 29. Tobasco I, Doering CR. 2017 Optimal wall-to-wall transport by incompressible flows. *Phys. Rev. Lett.* **118**, 264502. (doi:10.1103/PhysRevLett.118.264502)
- 30. Doering CR, Tobasco I. 2019 On the optimal design of wall-to-wall heat transport. *Commun. Pure Appl. Math.* **72**, 2385–2448. (doi:10.1002/cpa.21832)
- 31. Motoki S, Kawahara G, Shimizu M. 2018 Maximal heat transfer between two parallel plates. *J. Fluid Mech.* **851**, R4. (doi:10.1017/jfm.2018.557)
- 32. Ding Z, Kerswell RR. 2020 Exhausting the background approach for bounding the heat transport in Rayleigh-Benard convection. *J. Fluid Mech.* **889**, A33. (doi:10.1017/jfm.2020.41)
- 33. Souza AN, Tobasco I, Doering CR. 2020 Wall-to-wall optimal transport in two dimensions. *J. Fluid Mech.* 889, A34. (doi:10.1017/jfm.2020.42)
- 34. Whitehead JP, Doering CR. 2011 Ultimate state of two-dimensional Rayleigh–Bénard convection between free-slip fixed-temperature boundaries. *Phys. Rev. Lett.* **106**, 244501. (doi:10.1103/PhysRevLett.106.244501)
- 35. Wen B, Chini GP, Kerswell RR, Doering CR. 2015 Time-stepping approach for solving upper-bound problems: application to two-dimensional Rayleigh–Bénard convection. *Phys. Rev. E* **92**, 043012. (doi:10.1103/PhysRevE.92.043012)
- 36. Constantin P, Doering CR. 1999 Infinite Prandtl number convection. *J. Stat. Phys.* **94**, 159–172. (doi:10.1023/A:1004511312885)
- 37. Doering CR, Otto F, Reznikoff MG. 2006 Bounds on vertical heat transport for infinite-Prandtl-number Rayleigh–Bénard convection. *J. Fluid Mech.* **560**, 229–241. (doi:10.1017/S0022112006000097)
- 38. Plasting SC, Kerswell RR. 2003 Improved upper bound on the energy dissipation rate in plane Couette flow: the full solution to Busse's problem and the Constantin–Doering–Hopf problem with one-dimensional background field. *J. Fluid Mech.* 477, 363–379. (doi:10.1017/S0022112002003361)
- 39. Goluskin D, Doering CR. 2016 Bounds for convection between rough boundaries. *J. Fluid Mech.* 804, 370–386. (doi:10.1017/jfm.2016.528)
- 40. Childress S, Kerswell RR, Gilbert AD. 2001 Bounds on dissipation for Navier-Stokes flow with Kolmogorov forcing. *Physica D.* **158**, 105–128. (doi:10.1016/S0167-2789(01)00320-7)
- 41. Fantuzzi G, Goluskin D, Huang D, Chernyshenko SI. 2016 Bounds for deterministic and stochastic dynamical systems using sum-of-squares optimization. *SIAM J. Appl. Dyn. Syst.* **15**, 1962–1988. (doi:10.1137/15M1053347)
- 42. Kerswell RR. 2001 New results in the variational approach to turbulent convection. *Phys. Fluids* **13**, 192–209. (doi:10.1063/1.1327295)
- 43. Bouillaut V, Flesselles B, Miquel B, Aumaître S, Gallet B. 2022 Velocity-informed upper bounds on the convective heat transport induced by internal heat sources and sinks. *Phil. Trans. R. Soc. A* 380, 20210034. (doi:10.1098/rsta.2021.0034)
- 44. Crighton DG, Gaster M. 1976 Stability of slowly diverging jet flow. J. Fluid Mech. 77, 397. (doi:10.1017/S0022112076002176)
- 45. Gaster M, Kit E, Wygnanski I. 1985 Large scales structures in a forced turbulent mixing layer. *J. Fluid Mech.* **150**, 23. (doi:10.1017/S0022112085000027)
- 46. Currie IG. 1967 Effect of heating rate on stability of stationary fluids. *J. Fluid Mech.* **29**, 337–347. (doi:10.1017/S0022112067000850)
- 47. Kerr OS, Gumm Z. 2017 Thermal instability in a time-dependent base state due to sudden heating. *J. Fluid Mech.* **825**, 1002–1034. (doi:10.1017/jfm.2017.408)
- 48. Goluskin D. 2016 Internally heated convection and Rayleigh-Bénard convection. New York, NY: Springer.
- 49. Spiegel EA. 1962 On the Malkus theory of turbulence. In *Mecanique de la Turbulence*, pp. 182–201, Paris: Centre National de la Recherche Scientifique.
- 50. Whitehead JP, Doering CR. 2012 Rigid bounds on heat transport by a fluid between slippery boundaries. *J. Fluid Mech.* **707**, 241–259. (doi:10.1017/jfm.2012.274)
- 51. Doering CR, Constantin P. 1996 Variational bounds on energy dissipation in incompressible flows. III. Convection. *Phys. Rev. E* **53**, 5957–5981. (doi:10.1103/PhysRevE.53.5957)
- 52. Otero J. 2002 Bounds for the heat transport in turbulent convection. University of Michigan: PhD thesis.

- 53. Ding Z, Wen B. 2020 A note on upper bound for heat transport in two-dimensional Rayleigh-Bénard convection. *Int. Commun. Heat Mass Transfer* **117**, 104785. (doi:10.1016/j.icheatmasstransfer.2020.104785)
- 54. O'Connor L, Lecoanet D, Anders EH. 2021 Marginally-stable thermal equilibria of Rayleigh-Bénard convection. *Phys. Rev. Fluids* **6**, 093501. (doi:10.1103/PhysRevFluids.6.093501)
- 55. Wen B, Chini GP, Dianati N, Doering CR. 2013 Computational approaches to aspect-ratio-dependent upper bounds and heat flux in porous medium convection. *Phys. Lett. A* 377, 2931–2938. (doi:10.1016/j.physleta.2013.09.009)
- 56. Wen B, Chini GP. 2018 Inclined porous medium convection at large Rayleigh number. *J. Fluid Mech.* 837, 670–702. (doi:10.1017/jfm.2017.863)
- 57. Goluskin D, Johnston H, Flierl GR, Spiegel EA. 2014 Convectively driven shear and decreased heat flux. *J. Fluid Mech.* **759**, 360–385. (doi:10.1017/jfm.2014.577)
- 58. Johnston H, Doering CR. 2009 Comparison of turbulent thermal convection between conditions of constant temperature and constant flux. *Phys. Rev. Lett.* **102**, 064501. (doi:10.1103/PhysRevLett.102.064501)
- 59. Kerr OS. 2016 Critical Rayleigh number for error function temperature profile with a quasi-static assumption. (http://arxiv.org/abs/1609.05124v2)
- 60. Tilgner A. 2017 Bounds on poloidal kinetic energy in plane layer convection. *Phys. Rev. Fluids* **2**, 123502. (doi:10.1103/PhysRevFluids.2.123502)
- 61. Tilgner A. 2019 Time evolution equation for advective heat transport as a constraint for optimal bounds in Rayleigh-Bénard convection. *Phys. Rev. Fluids* **4**, 014601. (doi:10.1103/PhysRevFluids.4.014601)
- 62. Fantuzzi G, Pershin A, Wynn A. 2018 Bounds on heat transfer for Bénard–Marangoni convection at infinite Prandtl number. *J. Fluid Mech.* **837**, 562–596. (doi:10.1017/jfm.2017.858)
- 63. Arslan A, Fantuzzi G, Craske J, Wynn A. 2021 Bounds on heat transport for convection driven by internal heating. *J. Fluid Mech.* **919**, A15. (doi:10.1017/jfm.2021.360)
- 64. Fantuzzi G, Wynn A. 2016 Optimal bounds with semidefinite programming: an application to stress-driven shear flows. *Phys. Rev. E* **93**, 043308. (doi:10.1103/PhysRevE.93.043308)

Downloaded from https://royalsocietypublishing.org/ on 25 April 2022

- 65. Fantuzzi G, Wynn A. 2015 Construction of an optimal background profile for the Kuramoto–Sivashinsky equation using semidefinite programming. *Phys. Lett. A* **379**, 23–32. (doi:10.1016/j.physleta.2014.10.039)
- 66. Ding Z, Marensi E. 2019 Upper bound on angular momentum transport in Taylor-Couette flow. *Phys. Rev. E* **100**, 063109. (doi:10.1103/PhysRevE.100.063109)
- 67. Lee H, Wen B, Doering CR. 2019 Improved upper bounds on the energy dissipation rate for shear flow with injection and suction. *Phys. Fluids* **31**, 085102. (doi:10.1063/1.5109059)